Ionics (2023) 29:3641–3652
https://doi.org/10.1007/s11581-023-05110-y

RESEARCH

# Electrochemical investigation of NiO@$MnO_2$@rGO ternary nanocomposite based electrode material for high-performance supercapacitor applications

**S. Seenivasan[1] · S. Dhinesh[2] · F. Maiz[3] · Mohd. Shkir[3,4]**

Received: 17 March 2023 / Revised: 4 June 2023 / Accepted: 28 June 2023 / Published online: 4 July 2023


**Abstract**
The task of designing multifunctional nanomaterials for high-performing electrochemical energy conversion and storage devices has proven to be extremely challenging. Here, we report the fabrication of a reduced graphene oxide (rGO)-based ternary nanocomposite NiO@$MnO_2$@rGO having a range of active sites for enhanced electrochemical activity. Powder-XRD, FE-SEM, TEM, and XPS techniques were used to analyze the prepared samples, revealing that the NiO@$MnO_2$@rGO nanocomposite had smooth cubic particles and 2D rGO nanosheets, with a particle size of 70 nm. The resulting nanostructure included a mesoporous backbone with NiO and $MnO_2$ NPs enclosed between rGO layers, featuring various active sites such as Ni, Mn, and carbon-based species. The novel NiO@$MnO_2$@rGO ternary nanocomposite material combines NiO, $MnO_2$, and rGO to achieve improved electrochemical performance in a cost-effective and scalable manner for supercapacitors. Notably, NiO@$MnO_2$@rGO modified structure exhibited excellent conductivity due to the presence of rGO, demonstrating a high charge storage capacity of 536 $Fg^{-1}$ at a current density of 1 $Ag^{-1}$. Furthermore, the nanocomposite displayed exceptional stability, with a capacitance retention of approximately 93% after 3000 cycles. These remarkable properties make the NiO@$MnO_2$@rGO nanocomposite a promising solution to meet future energy demands in a cost-effective manner, addressing the need for sustainable energy storage.

**Keywords** Ternary composites · Chemical oxidation states · Specific capacity · Cyclic stability

## Introduction

Due to the drastic growth of population, and increased industrial development, there are inadequate energy resources and enormous environmental issues. This can be overcome by an alternate option. Hence, this search led to the intensively developing and sensational topic, the 'supercapacitors' [1]. Supercapacitors are the upraising energy storage devices. They are known for their low internal resistance, higher rate of energy storage, and delivery with very high specific capacitance. In addition to that, they have high power density, longer life, are flexible, weightless, and have very less maintenance. There are three major components in a supercapacitor, which are electrodes, a separator, and an electrolytic solution since they work on the principle of electrochemical reaction. Among these components, choosing the exquisite electrode plays a vital role in the performance of the supercapacitor [2]. There are three categories of supercapacitors depending on the principle of energy storage. The primary type of supercapacitor is Electric Double Layer Capacitor, which is also called an EDLC supercapacitor. Here the energy is stored between the electrodes and the electrolytic solution called the Helmholtz double layer using electrostatic interaction. Generally, carbon materials are used as electrodes for EDLC supercapacitors [3].

The secondary type is the pseudocapacitors. Unlike EDLC, here charge transfers between the electrode and the electrolyte through the redox reaction. Active carbon, carbon fiber, carbon gel, and other porous carbon materials with high surface areas are frequently employed as electrode materials for EDLCs. The basic electrode used here is metal oxides and

✉ S. Seenivasan
seeni95physics@gmail.com

1 Department of Physics, Selvam College of Technology, Namakkal 637003, Tamilnadu, India

2 Department of Physics, Selvamm Arts & Science College (Autonomous), Namakkal 637003, Tamilnadu, India

3 Department of Physics, College of Science, King Khalid University, Abha 61413, Saudi Arabia

4 Division of Research and Development, Lovely Professional University, Phagwara, Punjab 144411, India

conducting polymers. The final category is the hybrid capacitor. This uses both the mechanism of EDLC and pseudocapacitors to achieve greater energy and power densities.

Further, the hybrid is grouped into three different kinds based on the electrode used; asymmetric, composite, and battery-type hybrid supercapacitor. The suitable electrode materials for supercapacitors, such as $RuO_2$ and $IrO_2$, have high specific capacitance values and high cycle capacities, which has led to an increase in interest in this area [4, 5]. It has been determined that the local structures of hydrous ruthenium oxide with disordered structures maintaining easy transport paths are the reason why the capacitance can reach a high value of 720 $Fg^{-1}$. Despite these materials' exceptional performance, their high cost and toxicity prevent their widespread commercial use [6, 7]. In order to increase the rate capability of ruthenium oxide and lower its price, carbon materials have been added to it. However, because porous carbons have a lower density than hydrous ruthenium oxide, the resulting volume increase is not desired for small and light energy devices. $NiO_x$, $MnO_x$, $CoO_x$, and other alternatives have been developed recently as replacements for $RuO_2$ and $IrO_2$ in an effort to reduce the cost of electrode material while employing environmentally benign materials [8–10]. However, these inexpensive transition metal oxides exhibit smaller potential windows or poorer electrochemical-specific capacitance. As a result, numerous studies have been carried out to enhance these materials' capacitance performance, cycle capacity, and potential window [11].

Various materials possess notable electrochemical properties. For instance, metal–organic frameworks (MOFs) can be transformed into carbon materials with high surface area and porosity, resulting in improved electrochemical performance. $MX_2$ nanosheets, such as $MoS_2$ and $WS_2$, exhibit a layered structure, high electrical conductivity, and excellent electrochemical properties, showing promise for supercapacitor applications. When $MX_2$ nanosheets are combined with carbon materials like graphene or carbon nanotubes, they synergistically enhance the electrical conductivity and charge storage capacity of supercapacitor electrodes. MXenes, such as $Ti_3C_2Tx$, possess high surface area, good electrical conductivity, and excellent capacitance, making them suitable for high-performance supercapacitors [12–14]. Integrating $MX_2$ nanosheets with conducting polymers like polyaniline or polypyrrole enhances the charge storage capacity and cycling stability of supercapacitor electrodes. The combination of MOFs and carbon nanotubes improves electrical conductivity and pore accessibility, leading to enhanced supercapacitor performance. Hybrid structures of graphene and $MX_2$ materials exhibit high electrical conductivity, large surface area, and efficient charge transfer, resulting in the superior performance of supercapacitor electrodes. Incorporating MOFs into metal oxide structures like $Co_3O_4$ or NiO improves capacitive behavior, stability, and ion diffusion kinetics [15]. Hybrid structures combining $MX_2$ nanosheets and graphene oxide demonstrate synergistic effects, leading to improved charge storage capacity and cycling stability in supercapacitor electrodes.

$NiO@MnO_2@rGO$ offers several advantages compared to other materials. The combination of NiO, $MnO_2$, and rGO creates a synergistic effect, where each component contributes unique properties like high specific capacitance, improved electrical conductivity, and enhanced structural stability. NiO and $MnO_2$ exhibit high theoretical capacitance and pseudocapacitive behavior, while rGO provides a conductive framework for efficient charge transfer, resulting in enhanced energy storage capacity [16–18]. Incorporating rGO in the $NiO@MnO_2$ composite mitigates volume changes and structural degradation during charge–discharge cycles, leading to improved cycling stability and extended electrode lifespan [19, 20]. The presence of rGO facilitates rapid ion diffusion and electrolyte penetration, enhancing the charge–discharge rate capability [21–23]. Overall, the combination of NiO, $MnO_2$, and rGO provides a larger surface area, enabling more active sites for electrochemical reactions and promoting efficient utilization of the electrode material.

Due to its high electrochemical performance, eco-friendliness, and inexpensive cost, nickel oxide seems to be a prospective electrode material for pseudocapacitors [24]. It is commonly known that materials with nanostructures have unique and fascinating properties that are better than those of their bulk equivalents [25]. As a result, electrode materials for supercapacitors with nanoscale crystalline particle sizes would exhibit high specific surface areas, which lead to strong electrochemical activities and superior capacitive performance. Due to its physical and chemical features, manganese oxide ($MnO_x$) has attracted a lot of attention for use in electrochemical supercapacitors, ion exchange, catalysis, and other fields [26]. For electrochemical supercapacitors in particular, manganese oxide is regarded as the most promising electrode material because of its affordability, good electrochemical reactivity, and environmental compatibility. Carbon-based nanomaterials such as carbon nano-onions, carbon nanofibers, carbon nanotubes, reduced graphene oxide, graphene, and nitrogen (N) modified graphene are now regarded as excellent electroactive electrode nanomaterials that provide exceptional electrochemical properties for electrochemical capacitors [27, 28]. Because of its amazing electrical, thermal, and optical properties and wide range of applications, reduced graphene oxide has drawn the most attention of any of them. To enable high specific capacitance (CS) and cycling stability, NiO and $MnO_2$ morphologies and their composite with carbon structures/metal are heavily optimized. Recently, successful preparation of nickel oxide and manganese oxide has occurred [29]. The hydrothermal method is one of the chemical synthesis methods for the synthesis of nanostructured materials that are the easiest to regulate when compared to electrodeposition, the sol–gel technique, and template synthesis [30].

The literature evidence of rGO-wrapped metal oxide and its electrochemical performance is stated below. Youyi et al.

[31] chemically reduced graphene oxide (rGO) sheets during hydrothermal treatment and utilized them as a platform for the in-situ growth of $Co_3O_4$ nanoparticles with a size of 20 nm, resulting in the formation of an rGO–$Co_3O_4$ composite. In a two-electrode cell, the composite electrode exhibits a specific capacitance of 472 $Fg^{-1}$ when the scan rate is 2 mV/s. As the scan rate is increased to 100 mV/s, the composite retains 82.6% of its capacitance. Similarly, Wei et al. [32] put forward an environmentally friendly approach was utilized to prepare composites of reduced graphene oxide (rGO) and NiO. In this method, hydrogen gas was used as the reducing agent to convert the graphene oxide to its reduced form. The resulting NiO/rGO composite was employed as a hybrid capacitor electrode and exhibited excellent performance. At a discharge current density of 0.38 $Ag^{-1}$ in a 6.0 M KOH electrolyte, the composite achieved a maximum specific capacitance of approximately 428 $Fg^{-1}$. Li et al. [33] proposed a straightforward two-step synthesis approach devised to fabricate a fiber electrode composed of nitrogen-doped reduced graphene oxide (NGC), multi-walled carbon nanotubes (MWCNTs), and manganese dioxide ($MnO_2$) for flexible all-solid-state supercapacitors. The NGC/$MnO_2$-2 h fiber electrode demonstrated a higher specific capacitance of 367.7 $Fcm^{-3}$ at a current density of 0.5 $Acm^{-3}$ and exhibited outstanding cycling stability.

These reported works on rGO-wrapped metal oxide composites for supercapacitor electrodes lack detailed analysis of the long-term stability and degradation mechanisms, which are crucial for assessing their practical applicability. Additionally, the scalability and cost-effectiveness of the synthesis methods employed in these studies need to be further explored to enable large-scale production and commercial viability of these materials [34]. In contrast to the limitations mentioned in the reported works, the NiO@$MnO_2$@rGO nanocomposite addresses these concerns by providing insights into its long-term stability and degradation mechanisms. Extensive investigations on the electrochemical performance and structural integrity of the composite under various operating conditions are conducted, highlighting its potential for practical applicability. Furthermore, the synthesis method employed for NiO@$MnO_2$@rGO nanocomposite offers scalability and cost-effectiveness, paving the way for large-scale production and commercial viability. The novelty of this material lies in its synergistic combination of NiO, $MnO_2$, and rGO, which enables enhanced specific capacitance, improved electrical conductivity, and superior structural stability, making it a promising candidate for high-performance supercapacitor electrodes.

In this work, the NiO@$MnO_2$ was synthesized by hydrothermal technique, and the electrochemical performance was enhanced by the incorporation of reduced graphene oxide (rGO) in its lattice by ultrasonication method. The NiO@$MnO_2$@rGO ternary nanocomposite material is a cost-effective and promising option for supercapacitor electrodes. Unlike other review research works, it combines nickel oxide, manganese dioxide, and reduced graphene oxide to create a synergistic effect. The material's cost advantage stems from the abundance and affordability of NiO and $MnO_2$, while reduced graphene oxide offers a low-cost conductive additive. The scalable synthesis approach involves depositing NiO and $MnO_2$ onto reduced graphene oxide, ensuring good dispersion and interfacial contact. This simple process doesn't require specialized equipment or harsh conditions. The novelty lies in the unique combination of materials, with NiO providing high capacitance, $MnO_2$ offering cycling stability, and rGO enhancing electrical conductivity. As a result, the ternary nanocomposite demonstrates improved electrochemical performance, including higher specific capacitance, superior cycling stability, and excellent rate capability. Overall, the NiO@$MnO_2$@rGO ternary nanocomposite material stands out for its cost-effectiveness, scalable synthesis approach, and novel composition, making it a promising candidate for practical, low-cost supercapacitors.

## Materials

Nickel Nitrate hexahydrate (98%), Manganese Chloride (98%), Urea (99%), and Ammonium fluoride ($NH_4F$) (99%) were purchased from SRL Chemicals, India. All the reagents are used without any purification.

### *Synthesis of NiO and $MnO_2$ nanoparticles*

In the typical synthesis process, 0.1 M of nickel nitrate hexahydrate was dissolved in 30 mL of de-ionized water under constant stirring. Then 0.3 M of urea and 0.1 M of $NH_4F$ was dissolved in 30 mL of distilled water separately. The resultant solution was filled in a Teflon-lined stainless steel autoclave with a 100 mL capacity and heated at 180 °C for 20 h in a muffle furnace and allowed to cool until it attains room temperature. The obtained product was washed with water and ethanol and air dried at 80° in a hot air oven. Then the product was calcinated at 500 °C for 3 h and well-ground using a mortar and pestle to get NiO NPs. Similarly, the aforementioned procedure was carried out to synthesize the $MnO_2$ NPs.

### *Synthesis of NiO@$MnO_2$ nanocomposites*

The NiO@$MnO_2$ NC was synthesized by dissolving 0.1 M of as-synthesized NiO nanopowder and 0.1 M $MnCl_2.6H_2O$ in 30 mL of deionized water separately. Then 0.3 M $CH_4N_2O$ and 0.1 M $NH_4F$ were dissolved individually in 30 mL of deionized water. Then all the dissolved solutions were added to form a uniform mixture with the as-prepared NiO solution. Finally, the hydrothermal reaction was carried out at 180˚C for 20 h, and the resultant product was washed and calcined at 500˚C for 3 h to get NiO@$MnO_2$ NC.

### *Synthesis of NiO@$MnO_2$@rGO nanocomposites*

Briefly, 7 mg of the as-prepared NiO@$MnO_2$ NC and 3 mg of rGO powder were well grounded using mortar and pestle for 1 h, then transferred into the glass vial containing 30 mL of distilled water and bath sonicated for 2 h at 50 Hz. Then, the resultant suspension was centrifuged at 3000 rpm for 3 min and air dried at 80 °C for 3 h to get NiO@$MnO_2$@rGO NC.

## Results and discussions

### XRD analysis

The X-ray diffraction spectrum was obtained from an X'Pert PRO diffractometer using Cu $K_\alpha$ as radiating source of wavelength 1.5406 Å. The face-centered cubic structure of NiO NPs was confirmed and the five distinctive peaks at 2 $\theta$ values 37.16, 43.19, 62.90, 75.42, and 79.39 degrees are indexed to their hkl values (222), (400), (440), (622), and (444) respectively. Similarly, the XRD spectra of NiO@$MnO_2$ demonstrate the occurrence of well-defined intense sharp peaks positioned at 28.6, 37.16, 43.19, 56.7, 59.3, 62.9, 72.4, and 75.42 degrees corresponding to crystal planes of (110), (222), (400), (211), (220), (440), (301), and (622). In addition, the XRD pattern of NiO@$MnO_2$@rGO shows the increase in peak intensity owing to the incorporation of rGO into the NiO@$MnO_2$ lattice as shown in Fig. 1. The formation of NiO@$MnO_2$@rGO was perfectly agreed with the JCPDS card numbers 89–5881 and 81–226 [35, 36]. The average crystalline size of the NPs was calculated using Scherrer's Formula

$$D = \frac{k\lambda}{\beta cos\theta} \quad (1)$$

Here, k denotes the Scherrer's constant which is 0.94, $\lambda$ denotes the wavelength of the.

X-rays, $\beta$ represents the full-width half maximum (FWHM), $\theta$ is the diffraction angle. The average crystallite size was determined to be 32.18 nm.

### FTIR study

FTIR study reveals the diverse modes of vibration and their respective functional groups present in the NiO, NiO@$MnO_2$, and NiO@$MnO_2$@rGO NC. From FTIR spectra, the broad band centered at 3472 $cm^{-1}$ belongs to O–H stretching and they are hydrogen-bonded vibrations. The broadband that appears at 1682 $cm^{-1}$ arises owing to the bending of hydroxyl groups present in the interlayer water molecules [37]. The peak that appeared at 1452 $cm^{-1}$ is attributed to the O–H bending vibrations. Moreover, the two broad peaks present at 952, 861, and 664 $cm^{-1}$ attributed to the molecular vibrations of Ni–O, Mn–O, and Ni-Mn as shown in Fig. 2. Notably, no additional peaks were observed in FTIR spectra, which confirm the purity of the NiO, NiO@$MnO_2$, and NiO@$MnO_2$@rGO NC.

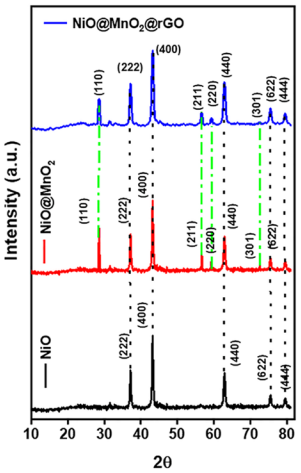


**Fig. 1** XRD spectrum of NiO, NiO@$MnO_2$, and NiO@$MnO_2$@rGO NC

### XPS analysis

The chemical state and purity of the NiO@$MnO_2$@rGO NC were evaluated using X-ray photoelectron spectroscopy (XPS) analysis. The survey spectrum (Fig. 3a) shows the existence of nickel, manganese, carbon, and oxygen in the NiO@$MnO_2$@rGO NC without any other additional impurities. Moreover, the core level spectrum of Ni 2p can be de-convoluted into Ni $2p_{3/2}$ and Ni $2p_{1/2}$ attributed to the binding energies of 854.7 eV and 871.8 eV and the existence of $Ni^{2+}$ and $Ni^{3+}$ states were also clearly observed as shown in Fig. 3b. Likewise, the high-resolution spectra of Mn reveals the peaks observed at the binding energies of 651.80 eV and 640.41 eV corresponds to the Mn $2p_{1/2}$ and Mn $2p_{3/2}$, respectively as shown in Fig. 3c. In addition, the presence of $Mn^{2+}$ and $Mn^{3+}$ states were also observed which may enhance the electrochemical behavior of the as fabricated electrode via offering sufficient electrons for redox process [38, 39]. The presence of C 1 s in the XPS spectrum (Fig. 3d), which was observed at the binding energy of 285.35, 284.13, 283.36, and 281.59 eV due to the availability of O-C=C, C–O–C/C=O, C-O, and C=C/C–C in the rGO matrix. The core level spectrum confirms the successful incorporation of rGO into the NiO@MnO NC lattice. Subsequently, the high-resolution spectra of O 1 s reveal three peaks at 532.17, 531.04, and 530.53 eV attributable to the C=O, $O_C$, and $O_L$. Moreover, $O_C$ and $O_L$ could be indexed to the chemically absorbed oxygen species and lattice oxygen bonded with metal atoms including Ni and Mn as evident from the Fig. 3e.

### SEM analysis

The morphology of NiO, NiO@$MnO_2$, and NiO@$MnO_2$@rGO NC was evaluated by SEM analysis. The SEM image

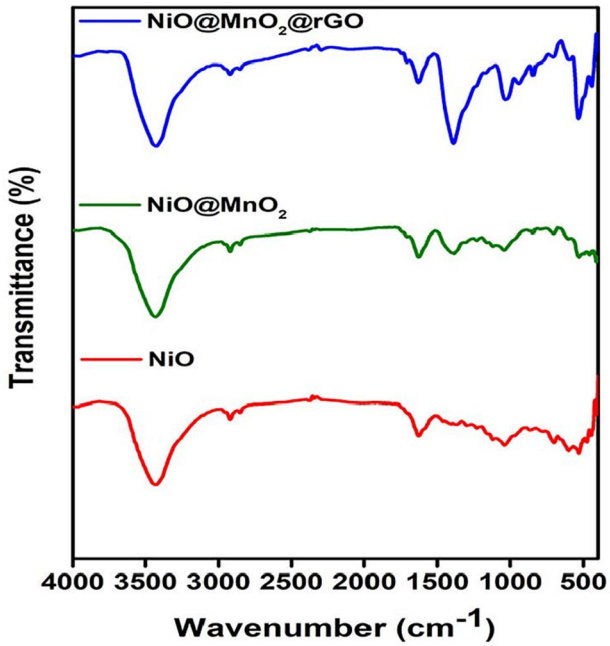


**Fig. 2** FTIR spectrum of NiO, NiO@$MnO_2$, and NiO@$MnO_2$@rGO NC

of NiO reveals the formation of cubic-shaped particles and the average particles size was found to be 80 nm (Fig. 4a). Similarly, the morphology of NiO@$MnO_2$ (Fig. 4b) shows the formation of cubic NiO particles was observed and in some regions, the $MnO_2$ particles with indefinite morphology were observed [40]. The average particle size of NiO@$MnO_2$ was identified to be 100 nm as shown in Fig. 4b. Likewise, the formation of cube-shaped particles and 2D rGO nanosheets were observed in NiO@$MnO_2$@rGO NC and the particle size was found to be 70 nm as shown in Fig. 4c. Notably, the morphology of NiO, $MnO_2$, and rGO was obtained for NiO@$MnO_2$@rGO NC which reveals that the large surface to volume ratio and provides enhanced electrochemical activity [41].

## TEM analysis

The particle size, morphology, and lattice spacing of the NiO@$MnO_2$@rGO NC were identified by High-Resolution Transmission Electron Microscope (HR- TEM). HR-TEM reveals the formation of cubic-shaped NiO@$MnO_2$@rGO particles with aggregated morphology and their particle size of about 75 nm as depicted in Fig. 5 (a-c). Moreover, the existence of rGO nanosheets in the NiO@$MnO_2$@rGO NC is visualized from the HRTEM analysis which confirms the successful incorporation into the NiO@$MnO_2$ lattice. Besides, the lattice spacing of NiO@$MnO_2$@rGO NC was found to be 0.326 nm corresponds to the plane (110) corresponds to the $MnO_2$ as shown in Fig. 5d. HRTEM confirms the uneven distribution of NiO, $MnO_2$ nanoparticles wrapped by the rGO nanosheets.

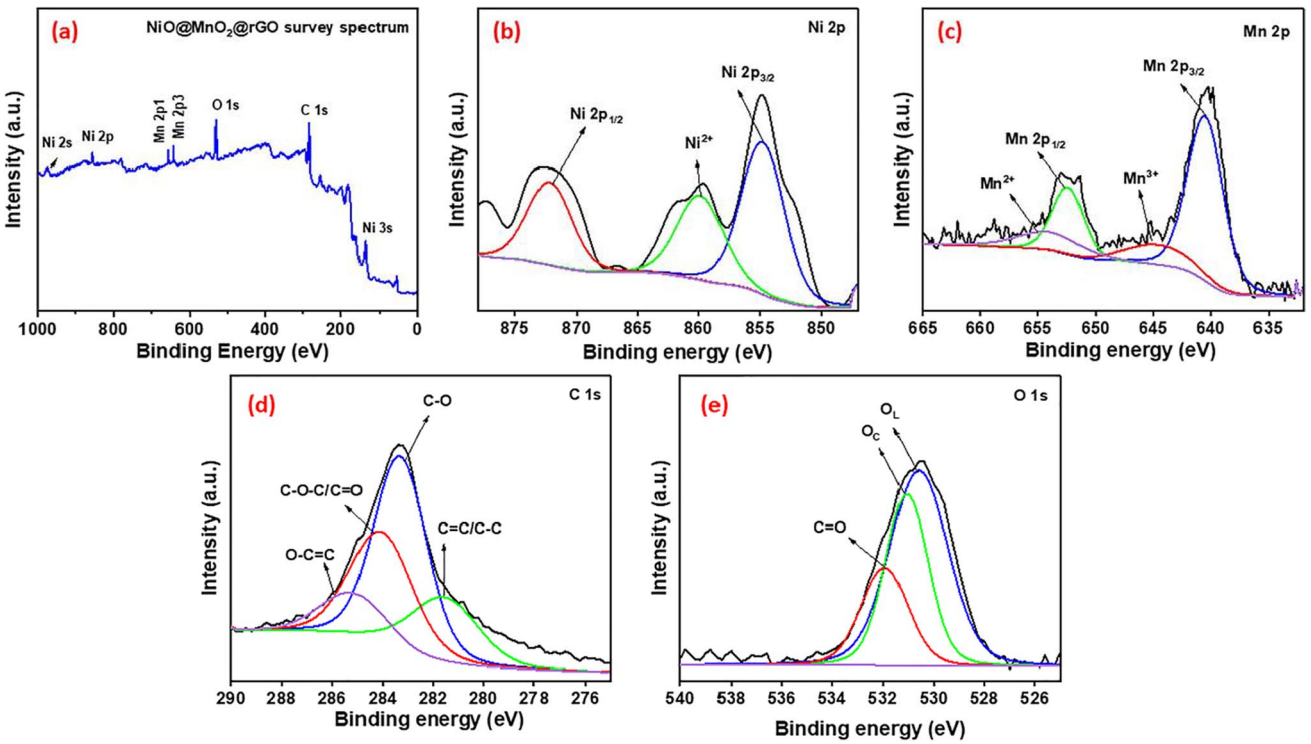


**Fig. 3** XPS spectrum (**a**) Survey spectrum, High-resolution spectrum of (**b**) Ni 2p, (**c**) Mn 2p, (**d**) C 1 s, and (**e**) O 1 s of NiO@$MnO_2$@rGO NC

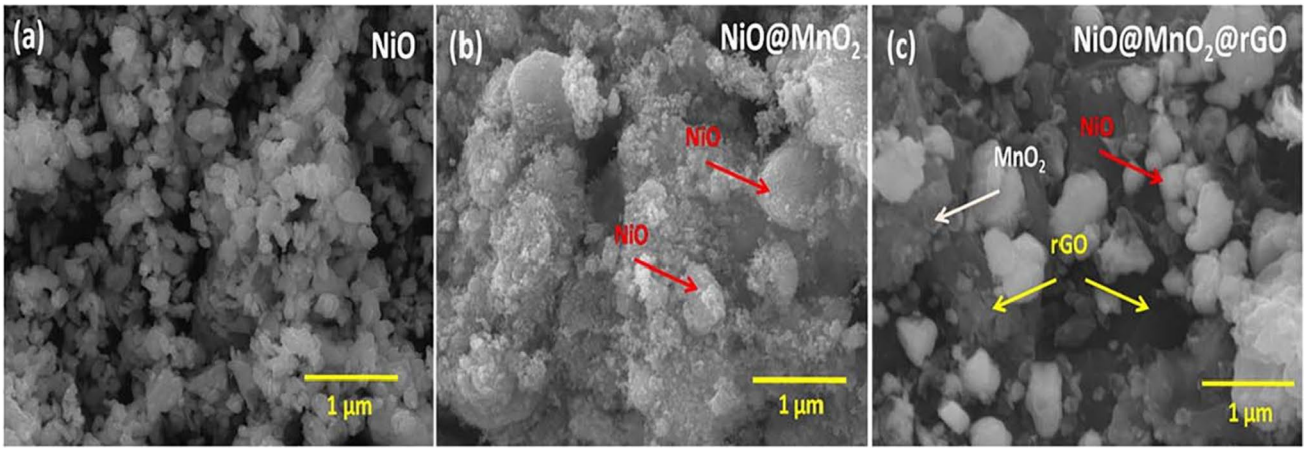


**Fig. 4** SEM image of (**a**) NiO, (**b**) NiO@$MnO_2$, and (**c**) NiO@$MnO_2$@rGO NC

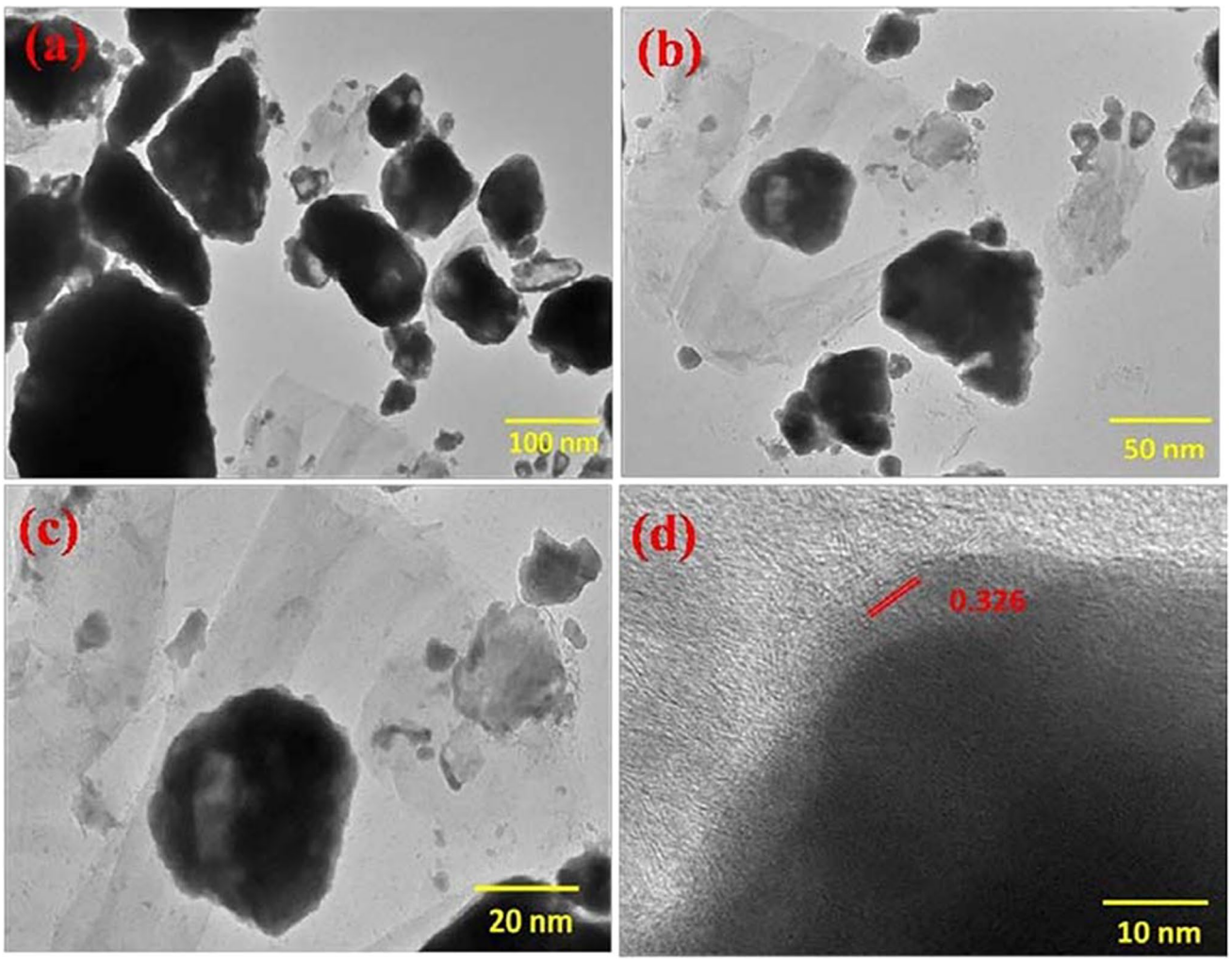


**Fig. 5** HR- TEM image of (**a-c**) NiO@$MnO_2$@rGO NC, and (**d**) lattice Spacing NiO@$MnO_2$@rGO NC

## Electrochemical studies

The electrochemical performance of the NiO, NiO@$MnO_2$, and NiO@$MnO_2$@rGO NC-based electrode materials was performed in 3 M of KOH electrolyte with Ag/AgCl and platinum wire as reference and counter electrodes respectively. CV analyses for NiO, NiO@$MnO_2$, and NiO@$MnO_2$@rGO were taken between 0–0.6 V potential range at diverse scan rates of 10, 25, 50, 100, and 200 mV/s. CV profile of all the samples reveals typical faradaic behavior, revealing their battery-like behavior and the charge storage at the electrode structure by sluggish redox process [42]. The specific capacitance of NiO was found to be 276, 238, 186.2, 145.48, and 129.02 $Fg^{-1}$ within the potential window of 0–0.6 V as shown in Fig. 6a. Similarly, the specific capacitance for NiO@$MnO_2$ (Fig. 6b) was achieved to be 342.43, 287.1, 262.9, 231.76, and 202.3 $Fg^{-1}$ at the scan rates of 10–200 mV/s, revealing their enhanced electrochemical activity due to the synergistic effect of NiO and $MnO_2$ [43]. Likewise, the specific capacitance of NiO@$MnO_2$@rGO was 536, 482, 438, 382, and 343 $Fg^{-1}$ at the scan rate of 10–200 mV/s as shown in Fig. 6c. This superior electrochemical activity is due to the synergistic effect of NiO and $MnO_2$ and the existence of rGO in the composite providing the combined charge storage process of both the EDLC and Faradaic process. The appreciable shift in oxidation and reduction peaks proves the battery-like nature of the fabricated NiO, NiO@$MnO_2$, and NiO@$MnO_2$@rGO electrodes, revealing their excellent rate capability. Also, the reversibility and stability of the electrode are good even at the higher scan rate [44].

The redox reactions of the electrode materials are as follows.

$$NiO + OH^- \leftrightarrow NiOOH + e^- \quad (2)$$

$$MnO + OH^- \leftrightarrow MnOOH + e^- \quad (3)$$

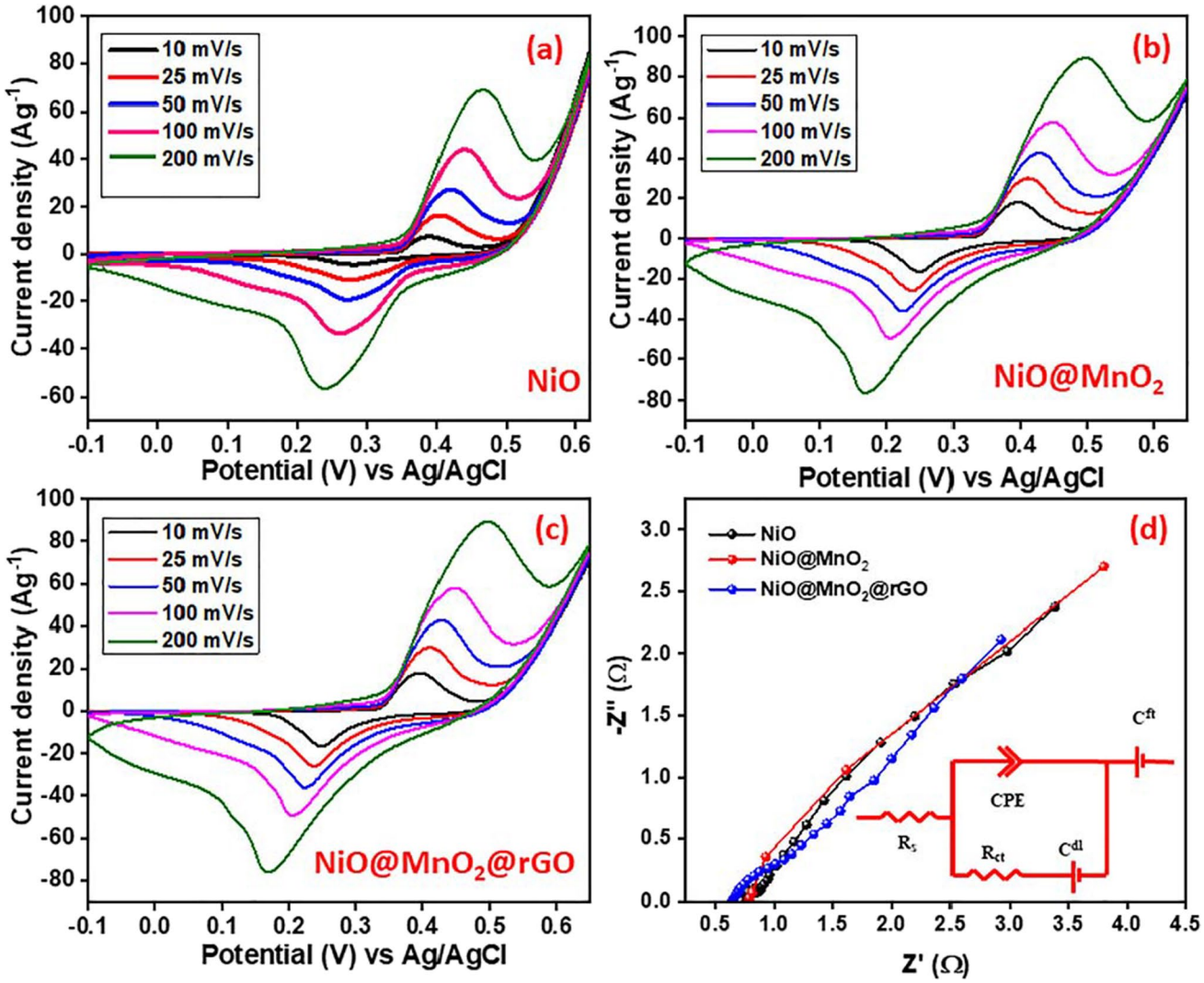


**Fig. 6** **a-c** CV spectrum at different scan rates (10–200 mV/s) and (**d**) EIS spectrum of NiO, NiO@$MnO_2$, and NiO@$MnO_2$@rGO

$$NiMnO + OH^- \leftrightarrow NiMnOOH + e^- \quad (4)$$

EIS analysis is used to study the impedance of the fabricated electrode. Here, the fabricated NiO, NiO@$MnO_2$, and NiO@$MnO_2$@rGO electrodes were analyzed over 100 kHz to 0.1 Hz range of frequency. A good supercapacitor electrode has lower impedance values of solution resistance ($R_s$) and charge transfer resistance ($R_{ct}$). To that, the $R_S$ and $R_{CT}$ of NiO@$MnO_2$@rGO are 0.415Ω and 0.054Ω, which is pretty lower than the impedance of the NiO $R_s = 1.1049Ω$ and $R_{ct} = 2.7014Ω$ and NiO@$MnO_2$ electrode, with $R_s = 0.82$ Ω and $R_{ct} = 2.42$ Ω as shown in Fig. 6d. The EIS spectrum has been fitted with equivalent circuit and inserted in the inset of Fig. 6d. The lower internal impedance of NiO@$MnO_2$@rGO shows the improved diffusion and excellent transport of electrons results in providing superior electrochemical activity [45, 46].

The charge and discharge rate of the electrode can be analyzed using Galvanostatic Charge Discharge analysis. The GCD analyses of NiO, NiO@$MnO_2$, and NiO@$MnO_2$@rGO were taken between the potential of 0–0.5 V and at the current densities of 1, 2, 3, 5, and 10$Ag^{-1}$ as shown in Fig. 7(a-c). The faradic behavior of the supercapacitor can be seen by the non-linear discharge curve which agrees well with the obtained CV profiles [47]. The discharge rate of NiO@$MnO_2$@rGO is higher than that of the NiO and NiO@$MnO_2$ indicating their excellent redox activity owing to the availability of numerous redox active sites and lower internal impedance [48, 49]. The obtained maximum specific capacitance of NiO was 236 $Fg^{-1}$ and for NiO@$MnO_2$, the specific capacitance was 320.3 $Fg^{-1}$ at the current density of 1 $Ag^{-1}$ respectively. In addition, the NiO@$MnO_2$@rGO shows enhanced specific capacitance of 510 $Fg^{-1}$ at 1 $Ag^{-1}$ which is higher when compared with the NiO and NiO@$MnO_2$. The cyclic stability of the NiO@$MnO_2$@rGO electrode (Fig. 7d) can be tested at the constant current density of 10 $Ag^{-1}$ which reveals the excellent stability of 92.8% even after 3000 charge–discharge cycles. Table 1 in

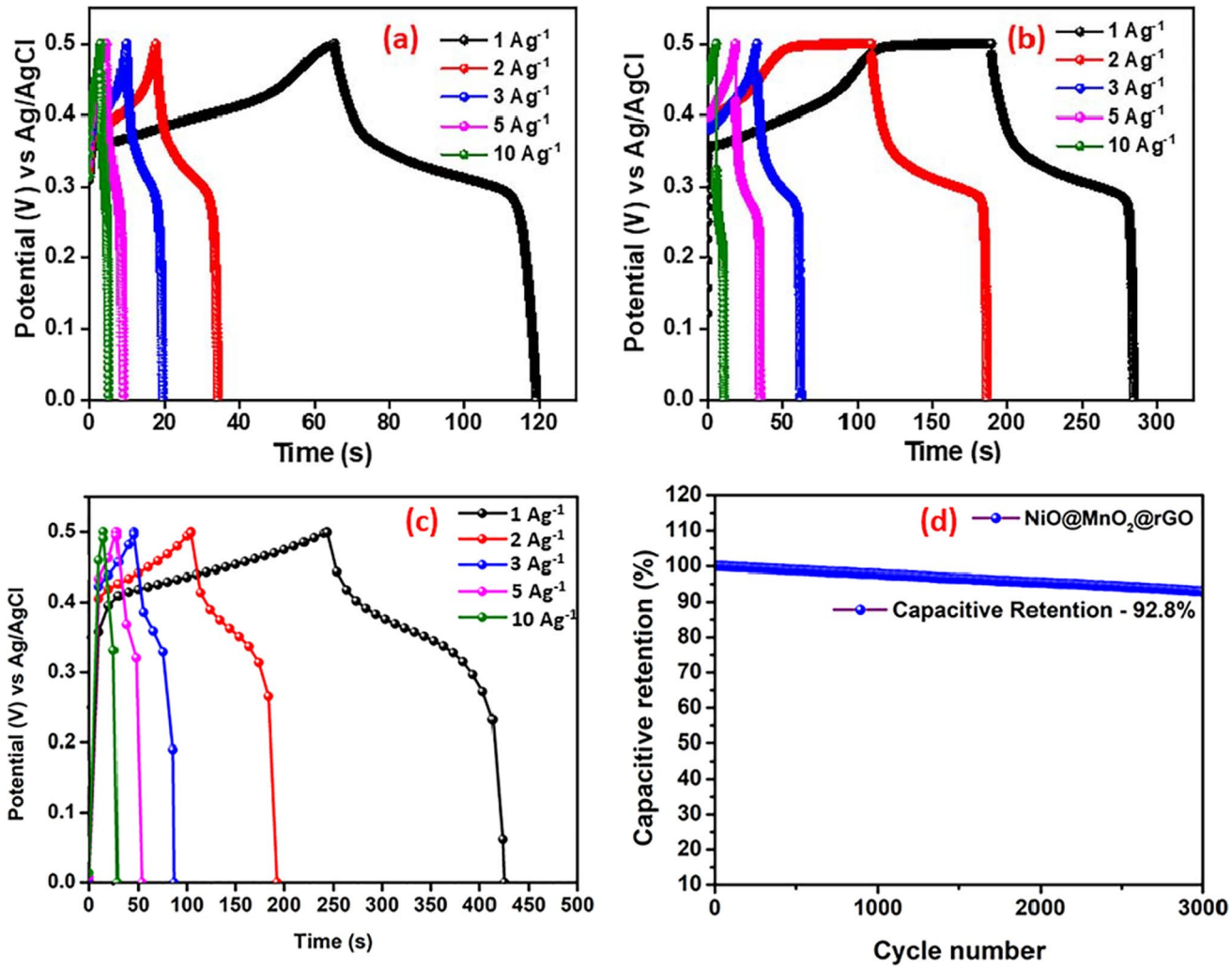


**Fig. 7** **a-c** GCD profile at the current density ranging from 1–10 $Ag^{-1}$ of NiO, NiO@$MnO_2$, and NiO@$MnO_2$@rGO NC, and (**d**) Capacitive retention of NiO@$MnO_2$@rGO for 3000 charge–discharge cycles

**Table 1** Comparison table with other rGO-wrapped literature findings with present work

| S.No | Composite | Synthesis method | Specific capacitance ($Fg^{-1}$) | Electrolyte | Cyclic stability | Ref. No |
|---|---|---|---|---|---|---|
| 1 | reduced-graphene-oxide-enclosed transition metal oxides (NiO/$Co_3O_4$) | Microwave irradiation method | 910 $Fg^{-1}$ (20 mV/s) | 0.1 M KOH | 89.9% after continuous 2000 cycles (100 mV/s) | [50] |
| 2 | reduced graphene oxide nanosheets anchored ZnO nanoparticles | Microwave irradiation | 102.4 $Fg^{-1}$ (30 mV/s) | 0.1 M KOH | 82.5% for 3000 cycles (100 mV/s) | [51] |
| 3 | reduced graphene oxide-wrapped manganese cobaltite ($MnCo_2O_4$) | Microwave-assisted approach | 562 $Fg^{-1}$ (20 mV/s) | 0.1 M KOH | 92.3% after 2000 cycles (100 mV/s) | [52] |
| 4 | $Ni(OH)_2$-ErGO@ NF electrode | Two step Electrochemical deposition | 3138 $Fg^{-1}$ (20 mV/s) | 1 M KOH | 88.6% after 3000 cycles (50 mV/s) | [53] |
| 5 | rGO@$Co_3O_4$/CoO hybrids | Single step microwave irradiation | 276.1 $Fg^{-1}$ (5 mV/s) | 0.1 M KOH | 82.37% capacitance retention after 10,000 cycles (60 mV/s) | [54] |
| 6 | NiO-$MnO_2$@rGO ternary hybrid | Microwave radiation | 165.7 $Fg^{-1}$ (20 mV/s) | 0.1 M KOH | 83.2% after 2000 continuous (100 mV/s) | [55] |
| 7 | rGO/CuO/PpPD | Hummers and In-situ polymerization | 512.12 $Fg^{-1}$ (1 $Ag^{-1}$) | 1 M $H_2SO_4$ | Capacitance retention of 92% after 10 000 cycles (10 $Ag^{-1}$) | [56] |
| 8 | CuO/rGO nanopellets | Coprecipitation method | 188 $Fg^{-1}$ (0.2 $Ag^{-1}$) | 1 M KOH | 96.3% capacity retention after 2000 charge–discharge cycles (1 $Ag^{-1}$) | [57] |
| 9 | rGO/CuO/Ag Ternary Nanocomposites | Hydrothermal approach | 575 $Fg^{-1}$ (1 $Ag^{-1}$) | 0.5 M $K_2SO_4$ | - | [58] |
| 10 | Z-CoO/RGO nanocomposite | In situ hydrothermal method | 275 $Fg^{-1}$ (1 $Ag^{-1}$) | 6 M KOH | 62% of initial capacitance after 1000 cycles (1 $Ag^{-1}$) | [59] |
| 11 | 3D macroporous ozonized RGO networks | Ozone treatment and thermal annealing | 239.4 $Fg^{-1}$ (1 $Ag^{-1}$) | 6 M KOH | 93.2% even up to 10,000 cycles (10 $Ag^{-1}$) | [60] |
| 12 | NiO@$MnO_2$@rGO nanocomposites | Hydrothermal and ultrasonication method | 510 $Fg^{-1}$ (1 $Ag^{-1}$) | 3 M KOH | 92.8% even after 3000 charge–discharge cycles (10 $Ag^{-1}$) | Present work |

the manuscript presents a comparison of recently reported studies on rGO-wrapped/deposited metal oxide composites with the findings of the present work, aiding in better comprehension.

## Conclusion

A facile hydrothermal technique was utilized to evaluate the electrochemical performance of NiO@$MnO_2$@rGO in 3 M KOH electrolyte. The XRD spectra reveal the structure, phase, crystallinity, and purity of the prepared material. From the CV curve, the maximum specific capacitance of NiO@$MnO_2$@rGO NC was found to be 536 $Fg^{-1}$ at the scan rate of 10 mV/s. From EIS spectra, the lower solution resistance ($R_s$) and charge transfer resistance ($R_{ct}$) of NiO@$MnO_2$@rGO were 0.415Ω and 0.054Ω respectively, and good capacitive behavior. Further, the fabricated electrode delivers excellent capacitive retention of about 92.8% for 3000 charge–discharge cycles. Thus, from the overall electrochemical performance, the NiO@$MnO_2$@rGO NC paved the way to solve future energy demands cost-effectively.

**Acknowledgements** The authors would like to express their appreciation to the Deanship of Scientific Research at King Khalid University for the financial support through research groups program under grant number R.G.P.2/298/44.

**Authors' contributions** S, Seenivaan: Investigation, Data curation, Writing—original draft. S. Dhinesh: Supervision, Conceptualization, Writing—Review & editing. F. Maiz: Writing—Review & editing, Mohd. Shkir: Conceptualization, Data Analysis, Software Investigation.

**Data availability** The data that has been used is confidential.

### Declarations

**Ethical approval** Ethical approval is not applicable.

**Competing interests** The authors declare that they have no known competing interests.

## References

1. Song X, Chen Q, Shen E, Liu H (2020) N-Doped 3D hierarchical carbon from resorcinol–formaldehyde–melamine resin for high-performance supercapacitors. New J Chem 44(20):8638–8649
2. Gonçalves JM, da Silva MI, Toma HE, Angnes L, Martins PR, Araki K (2020) Trimetallic oxides/hydroxides as hybrid supercapacitor electrode materials: a review. J Mater Chem A 8(21):10534–10570
3. Li L, Zhang YQ, Liu XY, Shi SJ, Zhao XY, Zhang H, Ge X (2014) One-dimension MnCo2O4 nanowire arrays for electrochemical energy storage. Electrochim Acta 116:467–474
4. Deshmukh AD, Urade AR, Nanwani AP, Deshmukh KA, Peshwe DR, Sivaraman P, Dhoble SJ, Gupta BK (2018) Two-dimensional double hydroxide nanoarchitecture with high areal and volumetric capacitance. ACS omega 3(7):7204–7213
5. Samdani KJ, Park JH, Joh DW, Lee KT (2018) Self-assembled Bi2MoO6 nanopetal array on carbon spheres toward enhanced supercapacitor performance. ACS Sustain Chem Eng 6(12):16702–16712
6. Halder L, Maitra A, Das AK, Bera A, Karan SK, Paria S, Bera A, Si SK, Khatua BB (2019) Fabrication of an advanced asymmetric supercapacitor based on three-dimensional copper–nickel–cerium–cobalt quaternary oxide and GNP for energy storage application. ACS Appl Electron Mater 1(2):189–197
7. Shendkar JH, Jadhav VV, Shinde PV, Mane RS, Dwyer CO (2018) Hybrid composite polyaniline-nickel hydroxide electrode materials for supercapacitor applications. Heliyon 4(9):e00801
8. Zhou W, Liu X, Sang Y, Zhao Z, Zhou K, Liu H, Chen S (2014) Enhanced performance of layered titanate nanowire-based supercapacitor electrodes by nickel ion exchange. ACS Appl Mater Interfaces 6(6):4578–4586
9. Singh AK, Sarkar D, Karmakar K, Mandal K, Khan GG (2016) High-performance supercapacitor electrode based on cobalt oxide–manganese dioxide–nickel oxide ternary 1D hybrid nanotubes. ACS Appl Mater Interfaces 8(32):20786–20792
10. Dutta S, Pal S, De S (2019) Mixed solvent exfoliated transition metal oxides nanosheets based flexible solid state supercapacitor devices endowed with high energy density. New J Chem 43(31):12385–12395
11. Niu L, Wang Y, Ruan F, Shen C, Shan S, Xu M, Sun Z, Li C, Liu X, Gong Y (2016) In situ growth of $NiCo_2S_4$@ $Ni_3V_2O_8$ on Ni foam as a binder-free electrode for asymmetric supercapacitors. J Mater Chem A 4(15):5669–5677
12. Chen B, Song Q, Zhou Z, Lu C (2021) A novel sandwiched porous MXene/polyaniline nanofibers composite film for high capacitance supercapacitor electrode. Adv Mater Interfaces 8(12):2002168
13. Wang Y, Liu Y, Wang C, Liu H, Zhang J, Lin J, Fan J, Ding T, Ryu JE, Guo Z (2020) Significantly enhanced ultrathin NiCo-based MOF nanosheet electrodes hybrided with Ti3C2Tx MXene for high performance asymmetric supercapacitor. Eng Sci 9(12):50–59
14. Liu Y, Yu J, Guo D, Li Z, Su Y (2020) $Ti_3C_2Tx$ MXene/graphene nanocomposites: Synthesis and application in electrochemical energy storage. J Alloy Compd 30(815):152403
15. Xu P, Xiao H, Liang X, Zhang T, Zhang F, Liu C, Lang B, Gao Q (2021) A MXene-based EDA-$Ti_3C_2Tx$ intercalation compound with expanded interlayer spacing as high performance supercapacitor electrode material. Carbon 1(173):135–144
16. Kumar R, Sahoo S, Joanni E, Singh RK (2022) A review on the current research on microwave processing techniques applied to graphene-based supercapacitor electrodes: An emerging approach beyond conventional heating. J Energy Chem 74:252–282
17. Vadahanambi S, Jung JH, Kumar R, Kim HJ, Oh IK (2013) An ionic liquid-assisted method for splitting carbon nanotubes to produce graphene nano-ribbons by microwave radiation. Carbon 53:391–398
18. Kumar R, Singh RK, Dubey PK, Singh DP, Yadav RM, Tiwari RS (2015) Hydrothermal synthesis of a uniformly dispersed hybrid graphene–$TiO_2$ nanostructure for optical and enhanced electrochemical applications. RSC Adv 5(10):7112–7120
19. Kumar R, Sahoo S, Joanni E, Singh RK, Kar KK (2021) Microwave as a tool for synthesis of carbon-based electrodes for energy storage. ACS Appl Mater Interfaces 14(18):20306–25
20. Youssry SM, El-Hallag IS, Kumar R, Kawamura G, Tan WK, Matsuda A, El-Nahass MN (2022) Electrochemical deposition of uniform and porous Co–Ni layered double hydroxide nanosheets on nickel foam for supercapacitor electrode with improved electrochemical efficiency. J Energy Storage 50:104638
21. Kumar R, Singh RK, Vaz AR, Moshkalev SA (2015) Microwave-assisted synthesis and deposition of a thin ZnO layer on

microwave-exfoliated graphene: optical and electrochemical evaluations. RSC Adv 5(8):67988–67995
22. AbdElkodous M, El-Sayyad GS, Maksoud MA, Kumar R, Maegawa K, Kawamura G, Tan WK, Matsuda A (2021) Nanocomposite matrix conjugated with carbon nanomaterials for photocatalytic wastewater treatment. J Hazard Mater 410:124657
23. Kumar R, Youssry SM, Joanni E, Sahoo S, Kawamura G, Matsuda A (2022) Microwave-assisted synthesis of iron oxide homogeneously dispersed on reduced graphene oxide for high-performance supercapacitor electrodes. J Energy Storage 56:105896
24. Yu X, Sun J, Zhao W, Zhao S, Chen H, Tao K, Yaoping Hu, Han L (2020) MOF-derived $Bi_2O_3$@ C microrods as negative electrodes for advanced asymmetric supercapacitors. RSC Adv 10(24):14107–14112
25. Delbari SA, Ghadimi LS, Hadi R, Farhoudian S, Nedaei M, Babapoor A, Namini AS et al (2020) Transition metal oxide-based electrode materials for flexible supercapacitors A review. J Alloy Compd 857:158281
26. Zhang K, Lee TH, Noh H, Islamoglu T, Farha OK, Jang HW, Choi J-W, Shokouhimehr M (2019) Realization of lithium-ion capacitors with enhanced energy density via the use of gadolinium hexacyanocobaltate as a cathode material. ACS Appl Mater Interf 11(35):31799–31805
27. Mazinani B, Kazazi M, Mobarhan G, Shokouhimehr M (2019) The combustion synthesis of Ag-doped $MnCo_2O_4$ nanoparticles for supercapacitor applications. Jom 71(4):1499–1506
28. Zhang K, Lee TH, Khalilzadeh MA, Varma RS, Choi J-W, Jang HW, Shokouhimehr M (2020) Rendering redox reactions of cathodes in Li-ion capacitors enabled by lanthanides. ACS Omega 5(3):1634–1639
29. Zhang K, Kirlikovali KO, Le QV, Jin Z, Varma RS, Jang HW, Farha OK, Shokouhimehr M (2020) Extended metal–organic frameworks on diverse supports as electrode nanomaterials for electrochemical energy storage. ACS Appl Nano Mater 3(5):3964–3990
30. Long H, Shi T, Hu H, Jiang S, Xi S, Tang Z (2014) Growth of hierarchal mesoporous NiO nanosheets on carbon cloth as binder-free anodes for high-performance flexible lithium-ion batteries. Sci Rep 4(1):1–9
31. Sun Y, Zhang W, Li D, Gao L, Hou C, Zhang Y, Liu Y (2015) Facile synthesis of $MnO_2$/rGO/Ni composite foam with excellent pseudocapacitive behavior for supercapacitors. J Alloy Compd 15(649):579–584
32. Li W, Bu Y, Jin H, Wang J, Zhang W, Wang S, Wang J (2013) The preparation of hierarchical flowerlike NiO/reduced graphene oxide composites for high performance supercapacitor applications. Energy Fuels 27(10):6304–6310
33. Zhang L, Tian Y, Song C, Qiu H, Xue H (2021) Study on preparation and performance of flexible all-solid-state supercapacitor based on nitrogen-doped RGO/CNT/$MnO_2$ composite fibers. J Alloy Compd 5(859):157816
34. Rani B, Sahu NK (2020) Electrochemical properties of $CoFe_2O_4$ nanoparticles and its rGO composite for supercapacitor. Diam Relat Mater 1(108):107978
35. Guo W, Yu C, Li S, Wang Z, Yu J, Huang H, Qiu J (2019) Strategies and insights towards the intrinsic capacitive properties of $MnO_2$ for supercapacitors: challenges and perspectives. Nano Energy 57:459–472
36. Liu B, Liu B, Wang Q, Wang X, Xiang Q, Chen Di, Shen G (2013) New energy storage option: toward $ZnCo_2O_4$ nanorods/nickel foam architectures for high-performance supercapacitors. ACS Appl Mater Interfaces 5(20):10011–10017
37. Muthu RN, Tatiparti SSV (2020) Electrochemical behavior of cobalt oxide/boron-incorporated reduced graphene oxide nanocomposite electrode for supercapacitor applications. J Mater Eng Perform 29(10):6535–6549
38. Kandalkar SG, Gunjakar JL, Lokhande CD (2008) Preparation of cobalt oxide thin films and its use in supercapacitor application. Appl Surf Sci 254(17):5540–5544
39. Aadil M, Zulfiqar S, Shahid M, Haider S, Shakir I, Warsi MF (2020) Binder free mesoporous Ag-doped $Co_3O_4$ nanosheets with outstanding cyclic stability and rate capability for advanced supercapacitor applications. J Alloy Compd 844:156062
40. Lei S, Peng X, Liang Z, Li X, Wang C, Cheng B, Xiao Y, Zhou L (2012) Self-template formation and properties study of $Cr_2O_3$ nanoparticle tubes. J Mater Chem A 22(4):1643–1651
41. Xu X, Wu J, Yang N, Na H, Li L, Gao J (2015) $Cr_2O_3$: a novel supercapacitor electrode material with high capacitive performance. Mater Lett 142:172–175
42. Sharma M, Adalati R, Kumar A, Chawla V, Chandra R (2021) Single step fabrication of nanostructured $Cr_2O_3$-$MoO_2$ composite flexible electrode for top-notch asymmetric supercapacitor. Appl Surf Sci 555:149721
43. Maheshwaran G, Selvi C, Kaliammal R, Ramesh Prabhu M, Krishna Kumar M, Sudhahar S (2021) Exploration of $Cr_2O_3$-NiO nanocomposite as a superior electrode material for supercapacitor applications. Mater Lett 300:130191
44. Sivakumar P, Jana M, Kota M, Jung MG, Gedanken A, Park HS (2018) Controllable synthesis of nanohorn-like architectured cobalt oxide for hybrid supercapacitor application. J Power Sources 402:147–156
45. Shafi I, Liang E, Li B (2021) Ultrafine chromium oxide ($Cr_2O_3$) nanoparticles as a pseudocapacitive electrode material for supercapacitors. J Alloys Compd 851:156046
46. Liu F, Su H, Jin L, Zhang H, Chu X, Yang W (2017) Facile synthesis of ultrafine cobalt oxide nanoparticles for high-performance supercapacitors. J Colloid Interface Sci 505:796–804
47. Joseph S, Kempaiah DM, Benzigar M, Baskar AV, Talapaneni SN, Jhung SH, Park D-H, Vinu A (2017) Metal organic framework derived mesoporous carbon nitrides with a high specific surface area and chromium oxide nanoparticles for $CO_2$ and hydrogen adsorption. J Mater Chem A 5(40):21542–21549
48. Kandalkar SG, Dhawale DS, Kim C-K, Lokhande CD (2010) Chemical synthesis of cobalt oxide thin film electrode for supercapacitor application. Synth Met 160(11–12):1299–1302
49. Zhang M, Xiong Z, Jia J, Zhou Z, Botao Wu, Ni Y, Zhou X, Cao L (2020) Improving electrochemical performance of hollow $Cr_2O_3$/CrNnanoshells as electrode materials for supercapacitors. J Electroanal Chem 856:113696
50. Kumar R, Youssry SM, Soe HM, Abdel-Galeil MM, Kawamura G, Matsuda A (2020) Honeycomb-like open-edged reduced-graphene-oxide-enclosed transition metal oxides (NiO/$Co_3O_4$) as improved electrode materials for high-performance supercapacitor. J Energy Storage 30:101539
51. Kumar R, Youssry SM, Abdel-Galeil MM, Kawamura G, Matsuda A (2020) One-pot synthesis of reduced graphene oxide nanosheets anchored ZnO nanoparticles via microwave approach for electrochemical performance as supercapacitor electrode. J Mater Sci: Mater Electron 31:15456–65
52. Kumar R, Abdel-Galeil MM, Ya KZ, Fujita K, Tan WK, Matsuda A (2019) Facile and fast microwave-assisted formation of reduced graphene oxide-wrapped manganese cobaltite ternary hybrids as improved supercapacitor electrode material. Appl Surf Sci 481:296–306
53. Youssry SM, El-Nahass MN, Kumar R, El-Hallag IS, Tan WK, Matsuda A (2020) Superior performance of Ni $(OH)_2$-ErGO@NF electrode materials as pseudocapacitance using electrochemical deposition via two simple successive steps. J Energy Storage 30:101485
54. Kumar R, Sahoo S, Tan WK, Kawamura G, Matsuda A, Kar KK (2021) Microwave-assisted thin reduced graphene oxide-cobalt

oxide nanoparticles as hybrids for electrode materials in supercapacitor. J Energy Storage 40:102724
55. Kumar R, Matsuo R, Kishida K, Abdel-Galeil MM, Suda Y, Matsuda A (2019) Homogeneous reduced graphene oxide supported NiO-$MnO_2$ ternary hybrids for electrode material with improved capacitive performance. Electrochimica Acta 303:246–56
56. Eivazzadeh-Keihan R, Taheri-Ledari R, Mehrabad MS, Dalvand S, Sohrabi H, Maleki A, Mousavi-Khoshdel SM, Shalan AE (2021) Effective combination of rGO and CuO nanomaterials through poly (p-phenylenediamine) texture: utilizing it as an excellent supercapacitor. Energy Fuels 35(13):10869–10877
57. Lohar GM, Pore OC, Fulari AV (2021) Electrochemical behavior of CuO/rGO nanopellets for flexible supercapacitor, non-enzymatic glucose, and $H_2O_2$ sensing application. Ceram Int 47(12):16674–16687
58. Sridevi A, Balraj B, Senthilkumar N, Venkatesan GP (2020) Synthesis of rGO/CuO/Ag ternary nanocomposites via hydrothermal approach for opto-electronics and supercapacitor applications. J Supercond Novel Magn 33(11):3501–3510
59. Zha X, Wu Z, Cheng Z, Yang W, Li J, Chen Y, He L, Zhou E, Yang Y (2021) High performance energy storage electrodes based on 3D Z-CoO/RGO nanostructures for supercapacitor applications. Energy 1(220):119696
60. Bhattacharya P, Joo T, Kota M, Park HS (2018) CoO nanoparticles deposited on 3D macroporous ozonized RGO networks for high rate capability and ultralong cyclability of pseudocapacitors. Ceram Int 44(1):980–987